Available online at www.sciencedirect.com
SCIENCE DIRECT®
Carbon 42 (2004) 21–32
CARBON
www.elsevier.com/locate/carbon

Novel carbon nanofibers of high graphitization as anodic materials for lithium ion secondary batteries

Seong-Ho Yoon [a,*], Chul-Wan Park [b], Hojung Yang [a], Yozo Korai [a], Isao Mochida [a], R.T.K. Baker [c], Nelly M. Rodriguez [c]

[a] *Institute of Advanced Material Study, Kyushu University, Kasuga, Fukuoka 816-8580, Japan*
[b] *KETI, Masan-ri, Jinwi-myon, Pyungtaek-si, Kyunggi-do 451-865, South Korea*
[c] *Catalytic Materials Ltd, 1750 Washington Street, West Holliston, Holliston, MT 01746, USA*

Received 19 July 2002; accepted 15 September 2003

Abstract

Carbon nanofibers (CNFs) of high graphitization degree were prepared by a CVD process at 550–700 °C. They showed different structures according to catalyst and preparation temperatures. The structure of CNF prepared from CO/H_2 over an iron catalyst was controlled from platelet (P) to tubular (T) by raising the decomposition temperature from 550 to 700 °C. The CNFs prepared over a copper–nickel catalyst from C_2H_4/H_2 showed the typical herringbone (HB) structure regardless of the reaction temperatures. The CNFs prepared over Fe showed d_{002} of 0.3363–0.3381 nm, similar to that of graphite, indicating very high graphitization degree in spite of the low preparation temperature. Such CNFs of high graphitization degree showed high capacity of 297–431 mA h/g, especially in the low potential region. However, low first cycle coulombic efficiency of ≈60% is a problem to be solved. The graphitization of the CNF preserved the platelet texture, however, and formed the loops to connect the edges of the graphene sheets. Higher graphitization temperatures made the loop more definite. The graphitized CNF showed high capacity (367 mA h/g); however, its coulombic efficiency was not so large despite its modified edges by graphitization, indicating that the graphene edges were not so influential for the irreversible reaction of Li ion battery.

Keywords: A. Carbon nanotubes; B. Chemical vapor deposition; C. Transmission electron microscopy, X-ray diffraction; D. Electrochemical properties

1. Introduction

Carbonaceous materials have received considerable interest as anodic materials for use in lithium ion secondary batteries [1–15]. A number of carbonaceous materials have been investigated to find the best performances (large discharge capacity, small irreversible capacity or high coulombic efficiency, low discharge potential for obtaining high voltage), and low cost for mass production.

So far, graphitic carbons have been well established as an anodic material to be the intercalation host for lithium ions [16–18], although non-graphitic and non-graphitizable carbons such as glass-like carbon and semi-coke are still targets to improve further all of the anodic performances [19–21]. Their high reversible capacity and low discharge potential have been appreciated [2,3,5–10].

Graphitic materials are classified into two categories, natural and synthesized graphites. The former material is very cheap but its properties (except for high capacity) are not satisfactory, although it has been commercially used. Synthesized graphites such as graphitized mesocarbon microbeads (g-MCMB) and graphitized mesophase pitch based carbon fibers (g-MCF), have been also commercialized, being prepared from various anisotropic precursors through graphitization above 2800 °C. Such high temperature heat-treatment is considered as a major factor of high cost in mass production.

Recently, novel nanocarbons such as multi-walled carbon nanotubes (MWCNTs) and nanofibers with highly graphitic properties have been prepared through the catalytic decomposition of several hydrocarbons or carbon monoxide with hydrogen at 1100 °C [22]. So far

* Corresponding author. Fax: +81-92-583-7798.
E-mail address: yoon@cm.kyushu-u.ac.jp (S.-H. Yoon).

0008-6223/$ - see front matter © 2003 Elsevier Ltd. All rights reserved.
doi:10.1016/j.carbon.2003.09.021

MWCNTs have been studied in terms of their potential applications for the electrochemical storage of energy, especially for the anodic materials of lithium ion secondary batteries [23–28]. Nalimova et al. already proved that ≈2 Li atoms per C atom can be stored in MWCNTs under a high pressure of 6 GPa [23]. Gaucher et al. reported high degrees of irreversible (500 mA h/g) and reversible (450 mA h/g) insertion of lithium ion in aprotic medium due to the galvanostatic reduction–oxidation characteristics of MWCNTs, which were prepared from acetylene at 900 °C over Co supported on silica. A large hysteresis must be remarked in the extraction of lithium ion [24]. Wu et al. reported that CuO/MWCNTs could reversibly store 700 mA h/g [25]. They noticed that the structures of MWCNTs play important roles in both specific capacity, and cycle stability and that the capacity of less graphitized MWCNT was higher than that of the well graphitized MWCNT, whereas the latter exhibited better cycle stability and charge/discharge rates [26]. In spite of such interesting behaviors of carbon nanotubes and nanofibers as the host of lithium intercalation, their volumetric reversibility and high discharge potential relative to those of lithium metal are still not satisfactory for commercial applications [16–18]. Nevertheless, nanocarbons still appear promising to be anodic materials because of high graphitizability at lower temperature and lower cost for mass production.

Anodic performances of graphitized materials in lithium ion secondary batteries strongly depend, among other factors, on the degree of graphitization. The degree of graphitization is often estimated from the P_1-values [29], d-spacing (d_{002}) [5], Lc- or La-values [30] and the degree of turbostratic disorder [14], which are quantified by X-ray diffraction [31] or Raman spectroscopy [32]. Generally, X-ray crystallography is believed to provide such information on the average bulk structure, whereas Raman spectra give the relative population of the ordered (1580–1600 cm^{-1}) and disordered structure (1350–1380 cm^{-1}) at the surface. Both approaches have been recognized as not sufficient to evaluate the very high graphitization extent.

Recently, one of the present authors showed that the EVS (electrochemical voltage spectroscopy) [33,34] could differentiate the high degree of graphitization through detecting the staged charge/discharge process of lithium ion [35,36]. A series of constant potential steps are applied to an electrochemical cell and the cell is allowed to attain quasi-open-circuit conditions by letting the current decay to a preset threshold current ($I_{threshold}$). The charge accumulated in each potential step is integrated from the measured current and yields a $\Delta Q/\Delta V$ vs. V plot, where Q and V stand for specific capacity and potential vs. Li/Li^+, respectively. When both $I_{threshold}$ and potential step size can be controlled to be very small, the potential-charge relation is very close to the genuine thermodynamic data and the potential resolution is high. A particular advantage of this technique for the study of highly graphitized materials comes from the fact that the stage phenomena are involved in these materials during their electrochemical charge/discharge reactions and the coexistence of any phases is presented as a peak in the $\Delta Q/\Delta V$ vs. V plots. Therefore, even when highly graphitized materials show only a marginal difference in their degree of graphitization, the difference can be easily detected from the intensity and/or location of the highly resolved peaks.

A similar incremental capacity ($\Delta Q/\Delta V$ vs. V) plot can be obtained by taking the reciprocal derivative of V vs. Q curves which are provided by the galvanostatic charge/discharge cycling experiments. In this technique, a constant current is imposed on electrodes and the resulting potential (V)-capacity (Q) relation is presented. As this is a transient method, kinetic effects often obscure the resolution in the potential-capacity profiles unless the current is minimized.

In this report, the present authors aimed to measure the charge–discharge properties of novel carbon nanofibers (CNFs) of high graphitization extent prepared through a catalytic CVD process, using galvanometry and EVS methods. Three CNFs of different structure were prepared over iron, Cu–Ni and iron supported on alumina, and heat-treated at 2800 °C for further graphitization. Their microstructures were characterized with X-ray diffraction and high resolution transmission electron microscopy to define arrangement and stacking order of graphene sheets in the bulk of the fiber and their edge at the surface.

2. Experimental

2.1. Materials

The CNFs were prepared from the mixed gases of carbon monoxide and hydrogen or ethylene and hydrogen on non-supported iron and copper–nickel (Cu–Ni) catalysts in the temperature range 550–700 °C, using a conventional horizontal tube furnace. The iron catalyst powder used in this study was prepared through the precipitation of ferric carbonate by adding ammonium bicarbonate as described by Best and Russell [37]. The Cu–Ni catalyst powder was prepared through co-precipitation of cuprous and nickel carbonates using the same method. The precipitates were dried overnight in an oven at 100 °C and then calcined in air at 400 °C for 5 h to convert the carbonates into oxides. The calcined catalysts were reduced in 10% H_2/He mixture for 20 h at 480 °C. The reduced catalysts were subsequently cooled to ambient temperature in a helium atmosphere before being passivated in a 5% Air/He mixture for 1 h at room

temperature. The passivated catalysts were then removed from the reactor and stored for later use.

A quartz flow reactor for the preparation of CNF was heated in a conventional horizontal tube furnace. The gas flow to the reactor is precisely monitored and regulated with MKS mass flow controllers. Powdered catalyst (30 mg) was placed in a quartz boat at the center of the reactor tube in the furnace. After reduction in a 10% H_2/He mixture for 2 h at the prescribed temperature, helium was flushed for 0.5 h. The reactant gas of CO/H_2 or ethylene/H_2 mixture was then allowed to flow over the catalyst for 1 h. The total amount of carbon deposited for 1 h on stream was determined gravimetrically after the system was cooled to ambient temperature.

Prepared fibers were partially oxidized at the 450 and 600 °C for 30 min under the air flow (100 ml/min) using the same type of horizontal furnace to remove amorphous carbons on the CNF surface. CNF was also heat-treated at 2800 °C for 10 min for the further graphitization.

Commercial nanotube (H-fiber, SUN Nanotech Co. Ltd, China) and Brazilian natural graphite (BG, Natural crystalline graphite, Nacional de Grafite Co. Ltd, Brazil) were used as standard carbon materials.

Hydrogen (99.999%), carbon monoxide (99.9%) and He (99.99%) were obtained from MG industries and used without further purification. Reagent grade iron nitrate ($Fe(NO_3)_3 \cdot 9H_2O$), cuprous nitrate and nickel nitrate were obtained from Wako Chemical Co.

2.2. Sample characterization

Prepared CNFs were observed under a transmission electron microscope (JEOL JEM 200CX) equipped with a bio-scan camera and a high resolution transmission electron microscope (JEOL JEM-2001).

The crystallographic data were collected with an X-ray diffractometer (Rigaku Geigerflex, CuKα target) and the crystallographic parameters were calculated according to the Gakushin (JSPS) method [38].

Multi-point BET surface area was measured using a surface area analyzer (Coulter Omnisorb 100CX). Prior to this measurement, the CNFs were degassed at 150 °C for 8 h.

2.3. Electrochemical measurements

The galvanostatic charge/discharge and EVS were measured in a beaker-type three electrode cell, where Li metal foil was used as the counter and reference electrodes. The electrolyte used was 1 M $LiClO_4$ dissolved in ethylene carbonate and diethyl carbonate (1:1 in vol. ratio). Ten milligrams of CNF was mixed with 7 wt% of polymeric binder (polytetrafluoroethylene) and coated on a piece of copper exmet (long-width dimension = 0.2 mm, short-width dimension = 0.1 mm, size = 1×1 cm^2) to prepare the electrode. The molded carbon electrode was then dried at 120 °C under vacuum for at least 12 h before use. A gravimetric current density of 30 mA g^{-1} (equivalent to 0.3 mA cm^{-2}) was applied and the potential cut-off range was fixed at 0.0–2.0 or 0.0–3.0 V vs. Li/Li^+. The carbon electrodes were first charged (Li^+ intercalated) from 2.0 or 3.0 to 0.0 V and then discharged from 0.0 to 2.0 or 3.0 V without pausing. For the EVS measurements, an EG&G M362 scanning potentiostat/galvanostat and a programmable potential source were combined in order to control the applied potential step. The step was started at 10 mV from the open circuit of the fresh cells and then a sequential step was applied after the current decays down to 0.02 mA of the threshold. All the electrochemical experiments were carried out at ambient temperature in a glove box filled with argon (99.999%).

3. Results

3.1. Characterization of CNFs

Some physical properties of all CNFs prepared in this study are summarized in Table 1, where the preparation conditions are included.

The structure of CNF prepared from CO/H_2 over iron catalyst was controlled from platelet (P) to tubular (T) by raising decomposition temperatures from 550 to 700 °C, as shown in Fig. 1(a) and (b) by transmission electron microscopy. Fe 550 and Fe 600 which were prepared at 550 and 600 °C, respectively, showed always a platelet structure, whereas Fe 670 and Fe 670H prepared over 650 °C showed a tubular structure regardless of gas composition. The CNFs prepared at 700 °C carried deactivated catalyst nanoparticles encapsulated with several layers of graphene sheets. On the contrary, CNFs prepared over copper–nickel catalyst from the mixture of ethylene and hydrogen showed the typical herringbone (HB) structures regardless of the reaction temperature, as shown in Fig. 2. H-fiber (Commercial carbon nanotube) presumably prepared from the mixture of methane and hydrogen over iron supported on alumina showed relatively small diameters of $\approx$15 nm and hollow type fibril structure with HB-like texture.

Table 1 also shows elemental analyses of the CNFs. CNFs prepared over iron from CO/H_2 showed H/C values of 0.035–0.020, which were smaller than those of CNFs over Cu/Ni catalyst. The hydrogen content of the CNFs tended to increase with increasing hydrogen content in the feed gas. The graphitization of Fe 600 (g-Fe 600-2800) removed all hydrogen.

The BET surface areas of the CNFs are also summarized in Table 1. It is evident that the CNFs prepared over the iron catalyst had much lower surface areas than

Table 1
Preparation conditions and some physical properties of graphite nanofibers

Preparation conditions						Selected physical properties			
Catalyst	Sample ID	Temperature (°C)	Time (h)	Gas composition (CO/H_2, vol/vol)	Yield (GNFs/catalyst, wt/wt)	TEM	Elemental analyses	XRD	N_2-BET
						Structure	H/C (atomic ratio)	d_{002} (nm)	Surface area (m^2/g)
Fe	Fe 550	550	1	4/1	29	P[a]	–	0.3381	84
	Fe 600	600	1	4/1	16	P	0.035	0.3363	91
	Fe 670	670	1	4/1	20	T[b]	0.020	0.3363	65
	Fe 670H	670	1	1/4	8	T	0.025	0.3364	54
	Fe 700	700	1	4/1	11	D[c]	–	0.3363	–
	g-Fe 600-2800	600-graphitized at 2800	1 0.3[d]	4/1	16–90[e]	P	0.000	0.3363	28
Cu/Ni = 3/7 (wt/wt%)	CN 550	550	1	$C_2H_4/H_2 = 4/1$	70	HB[f]	0.082	0.3424	220
	CN 600	600	1	$C_2H_4/H_2 = 4/1$	68	HB	0.080	0.3412	180
Fe supported on alumina	H fiber (carbon nanotube)	950	?	CH_4/H_2	–	T	–	0.3450	350
Natural graphite	Brazilian graphite	–	–	–	–	–	0.000	0.3356	4

[a] Platelet structure.
[b] Tubular structure.
[c] Deactivated cells.
[d] Time for graphitization.
[e] Yield after graphitization.
[f] Herringbone structure.

those over copper–nickel or iron supported on alumina. Among the CNFs grown over the non-supported iron catalyst, tubular ones had lower surface area (54–60 m^2/g) than platelet CNFs (84–91 m^2/g). The surface area of graphitized g-Fe 600-2800 appeared much smaller than that of as-prepared Fe 600, as expected.

The XRD analyses of the CNFs are also summarized in Table 1. The interlayer spacing (d_{002}) of CNFs grown over iron catalyst was very small, 0.3363–0.3381 nm, similar to the value for natural graphite. The d-spacing of the g-Fe 600-2800 must be noted, 0.3363 nm, which is similar to that of the as-prepared Fe 600. The d-spacing of CN 600 was 0.3412 nm, a little smaller than that of CN 550 (0.3424 nm). Such d-spacings for CNFs prepared over Cu/Ni were larger than those of the CNFs prepared over Fe.

3.2. Structure of graphitized Fe 600

Fig. 3 shows TEM photographs of as-prepared and graphitized Fe-600s at 2000 and 2800 °C (g-Fe 600-2000 and g-Fe 600-2800). As-prepared Fe 600 clearly showed the platelet texture where the graphene sheets were strictly arranged perpendicular to the fiber surface and axis, the edges of the graphene sheets forming the surface. The graphitization preserved the platelet texture, but it formed the loops to connect the other edges of the graphene sheets. Higher graphitization temperature made the loops more definite. It is noted that two sheets formed the smallest loop.

3.3. Galvanostatic charge/discharge of as-prepared CNFs

Fig. 4(a) and (b) and Table 2 show the galvanostatic charge–discharge profiles, specific capacities and coulombic efficiencies recorded with CN 550, CN 600, Fe 550, Fe 600 and H-fiber. First of all, there is a definite difference in the shapes of the discharge profiles of CNFs examined in the present study. The discharge profiles of Fe 550 and Fe 600 showed definite plateaus in the voltage range 0.0–0.3 V vs. Li/Li^+, like Brazilian graphite, whereas CN 550, CN 600 and H-fiber did not or had a very small plateau, although CN 550 and CN 600 showed very large capacity of 1314–1338 and 601–852 mA h/g for charge and discharge, respectively. However, the discharge at 0.0–0.3 V vs. Li/Li^+ of CN 550 and CN 600, which was applicable for commercial Li-ion battery, was only 45 and 110 mA h/g. In contrast, Fe 550 and Fe 600 showed the larger discharge capacity of 175–278 mA h/g at 0.0–0.3 V vs. Li/Li^+, like Brazilian natural graphite, although their total capacities were 575–718 and 363–423 mA h/g for charge and discharge, respectively. Fe 600 showed a considerable discharge at 0.3–1.2 V vs. Li/Li^+, which is often observed with non-

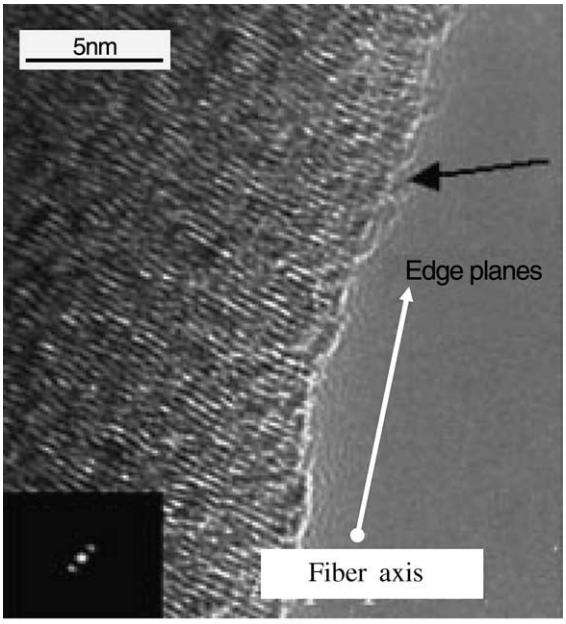

(a)

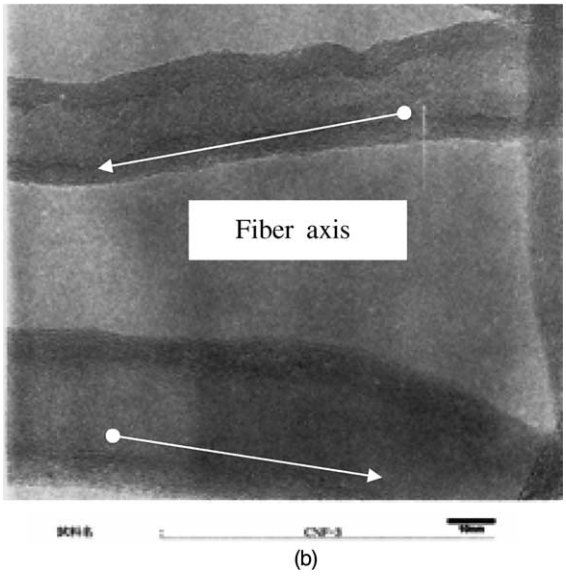

(b)

Fig. 1. HR-TEM photographs of Fe catalytic CNFs (a) Fe 600, (b) Fe 670 H.

graphitized carbon [35]. H-fiber showed very large charge capacity of 2182 mA h/g while discharge capacity was only 535 mA h/g. The discharge capacity at 0.0–0.3 V vs. Li/Li$^+$ was as small as 92 mA h/g.

Fig. 5(a) and (b) and Table 2 show the whole charge and discharge profiles, capacities and the first cycle coulombic efficiencies of CNFs prepared on the iron catalyst. All CNFs showed values of 493–718 and 297–423 mA h/g in charge and discharge, respectively, which was larger than the theoretical charge value for graphite single crystal (372 mA h/g). Plateaus in the discharge profiles of Fe 550, Fe 600, Fe 670, Fe 670H, and Fe 700 at 0.0–0.3 V vs. Li/Li$^+$ increased with increasing prep-

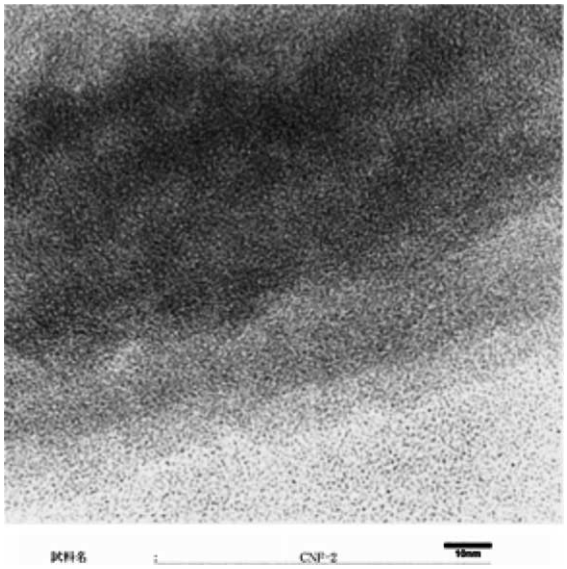

Fig. 2. HR-TEM photograph of CN 600 CNF.

aration temperature, reached a maximum at 670 °C and then decreased. Sample Fe 670 showed a larger plateau than Fe 670H. Another unique discharge profile was observed with Fe series CNFs. The capacity at 0.3–3.0 V vs. Li/Li$^+$ was 100–160 mA h/g, which has been conjectured as discharges in the non-graphitic portions of Fe CNFs. The capacity at 0.3–3.0 V vs. Li/Li$^+$ usually decreases with increasing degree of graphitization of carbon materials.

Fig. 6 showed the discharge profiles of samples PO450 and PO600 which were obtained by oxidation of Fe 600 to 0.5 and 30% burn-off, respectively. PO450 showed a very increased capacity of 301 mA h/g up to 0.3 V, whereas PO600 failed to show any capacity increase.

3.4. Galvanostatic charge/discharge of graphitized CNFs

Fig. 7(a) shows the charge profiles of Fe 600 and its graphitized CNFs (g-Fe 600-2000, g-Fe 600-2800). The first charge profiles showed some reaction at ≈0.8 V. The plateaus at ≈0.8 V showed no large difference although they became smaller with the increase of graphitization temperature.

Fig. 7(b) and (c) shows the discharge profiles of Fe 600, graphitized Fe 600s and Brazilian graphite. The discharge capacity up to 0.3 V increased with the graphitization temperature. Sample Fe 600 showed 278 mA h/g, whereas g-Fe 600-2000 and g-Fe 600-2800 showed 300 and 324 mA h/g, respectively. The increase of capacity by graphitization was very limited, presumably because of the high graphitization degree of the as-prepared CNF. Brazilian graphite showed the typical discharge profiles of graphite, which reflected stepwise de-intercalation of Li-ion inserted into the graphite

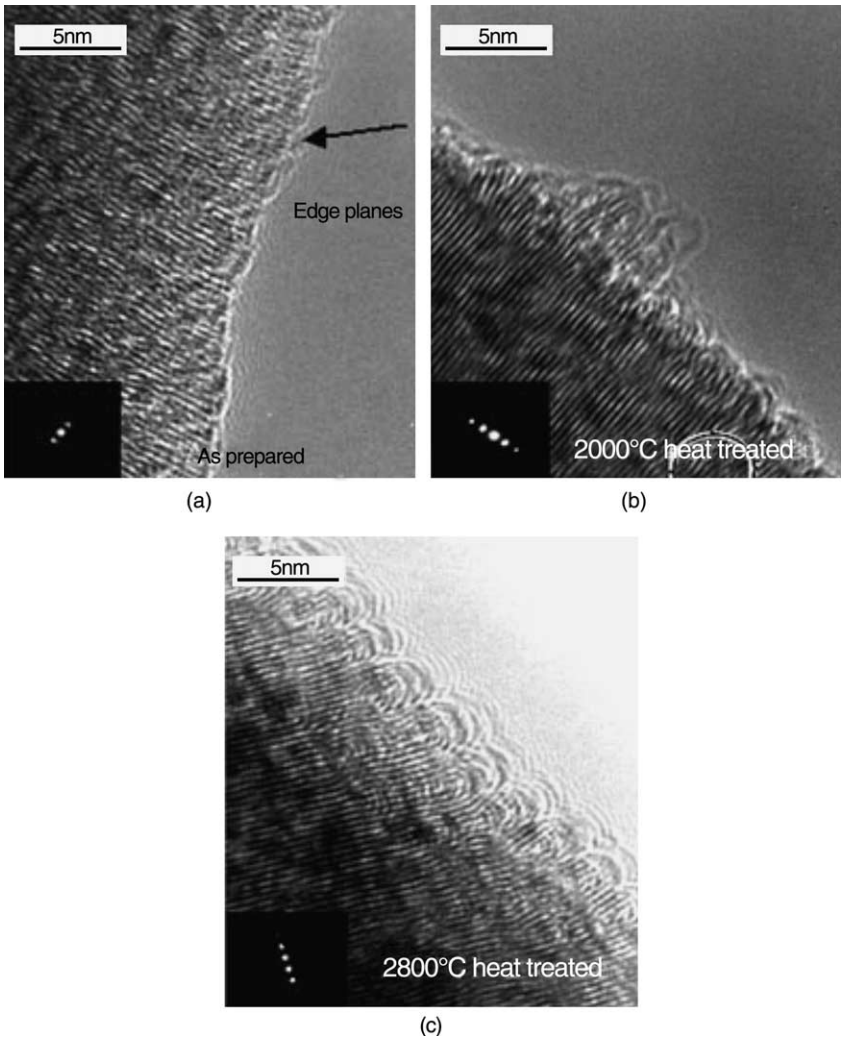

Fig. 3. HR-TEM photographs of (a) Fe 600 (b) Fe 600-2000 and (c) Fe 600-2800.

layers. Sample g-Fe 600-2800 showed basically the same profile which carried a somewhat smaller plateau, showing a small 2 + 2L stage and a larger 1 + 2 stage [39].

3.5. EVS measurements

Fig. 8 shows the charge and discharge EVS profiles of Fe series CNFs and Brazilian graphite at 0.0–1.0 V vs. Li/Li^+. Sample Fe 550 showed its charge in the whole range and less separated peaks of the stages. The EVS profile of Fe 600 appeared to give superimposed peaks labeled B, and C. Such a superposition disappeared by preparation above 600 °C or by graphitization. Another peak labeled A was observed in the charge profile of Fe 550. The A peak disappeared in the charge profiles of Fe 600, Fe 670, Fe 700, and g-Fe 600 and was removed by partial oxidation at 450 °C. Soot-like carbon on Fe 550 may cause such a peak.

Although sample Fe 550 discharged over the whole potential range, a higher preparation temperature moved the initial discharge potential in the positive direction, the discharge capacity at 0.05–0.25 V becoming dominant above 600 °C. In contrast to the galvanostatic discharge profiles (Fig. 7), the staged discharge was clearly identified as peaks in the EVS profiles of Brazilian graphite and highly graphitized CNFs. It must be noted that two experiments scanned the full potential range (0.0–2.0 V) in the same period (10 h). The EVS profiles distinguished clearly the respective peaks with all Fe 550, Fe 600, Fe 670, and Fe 700 CNFs which were observed at similar potentials in the corresponding galvanostatic profiles in Fig. 5. The peak separation, which reflected the stage discharges, became more apparent with Fe 600, which showed at least three peaks. The profiles of CNFs prepared above 600 °C became eventually closer to that of Brazilian graphite except for the transition peak from the dilute first stage to the fourth stage.

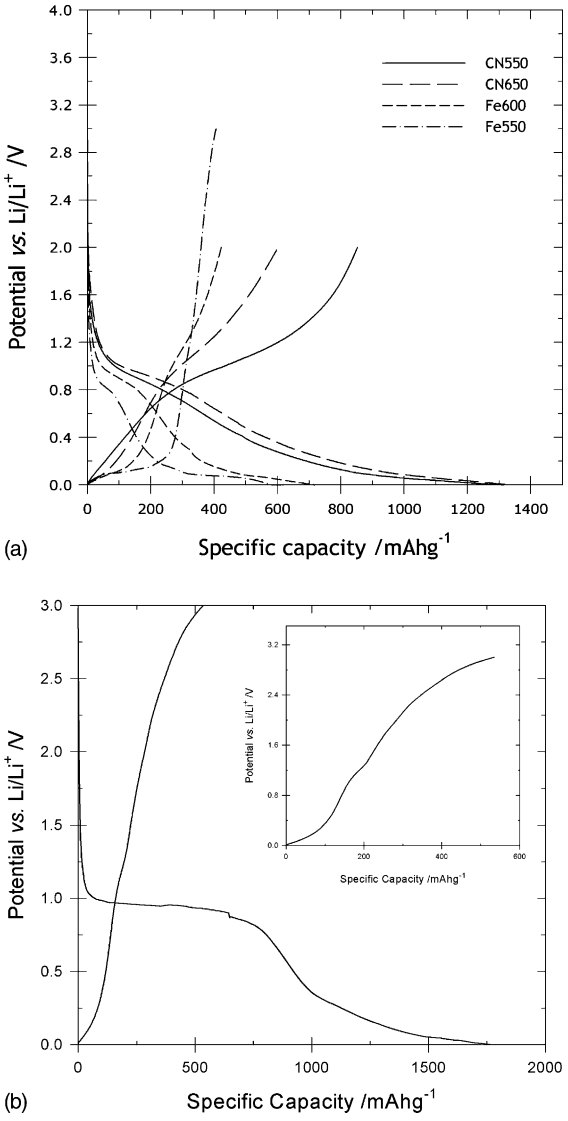

Fig. 4. Galvanostatic charge and discharge profiles of (a) CN550, CN650, Fe 550 and Fe 600 CNFs (b) Hyperion CNF. The measurements were made with a gravimetric current density of 30 mA g^{-1} (equivalent to 0.3 mA cm^{-2}) in the potential range of 0.0–3.0 V (vs. Li/Li^+).

Charge and discharge profiles in EVS were basically corresponding to each other. The intensity decrease of the peak and a shift to negative potential with reduced intensity were observed at higher temperature. A more careful inspection of the profiles indicates some delicate differences between the charge and discharge profiles.

Three features can be observed in the discharge profiles in EVS. Three peaks were observed in the discharge profiles of Fe 600, which are a well distinct peak A near 0.03 V, a completely separated peak of C and a new peak at 0.2 V. The discharge peak at about 0.03 V was common to non-graphitizable (disordered or hard) carbonaceous materials heat-treated at 1000–1400 °C [29]. This sample had some amorphous carbon on the surface of CNFs. Such a peak was weakened or disappeared in the profiles of samples Fe 670, Fe 670H and Fe 700.

The second feature of the discharge profiles of the Fe series was that Fe series (except for Fe 550) showed good peak separation at 0.05–0.25 V in the EVS profiles that were associated with the highly developed graphite structure of CNFs. Sample Fe 550 showed some peaks separated but not completely, once again illustrating its relatively low graphitization extent.

For a better insight into the graphitization extent of Fe series fibers, the discharge EVS profiles of Fe 600 and g-Fe 600-2800 were compared with that of Brazilian graphite: the latter provided a much closer profile to that of Brazilian graphite. Peak A observed with Fe 600 disappeared while peak E which reflected the transition from the dilute first stage to the fourth stage seen in sample g-Fe 600-2800. Thus sample g-Fe 600-2800 is concluded to be very graphitized.

4. Discussion

The present study reported the following findings.

(1) CNFs with particular arrangements of graphene sheets along the fiber were successfully and selectively prepared by selecting the catalyst and controlling the preparation temperature.
(2) The CNFs of the present study are basically very graphitic, the extent of graphitization depending on the preparation temperature whereby the arrangement was also controlled.
(3) Some CNFs show charge–discharge profiles typical of graphite as a lithium ion battery anode.

Correlations between structure and anodic performance of CNFs can now be discussed.

4.1. Structure and anodic performance of as-prepared CNF

All CNFs prepared over iron in the present study are carbons of high graphitization in terms of d_{002}. The largest total charge and discharge capacities were obtained with sample Fe 670, which had a tubular arrangement of graphene sheets. However, among the as-prepared CNFs without the graphitization treatment, the largest discharge capacity in the potential range 0.0–0.3 V vs. Li/Li^+ that is important for the real Li ion battery was found with Fe 600-PO450, which had a platelet arrangement of graphene sheets. The discharge capacity in the potential range 0.0–0.3 V vs. Li/Li^+ is very important because the difference of the discharge potentials of cathode and anode is available in the Li ion battery system. The fact that partial oxidation at 450 °C increased discharge capacity in the potential range

Table 2
Capacities and coulombic efficiency of graphite nanofibers used in this study

Samples		Capacities (mA h/g)		Coulombic efficiency (%)
Sample ID	After-treatment	Charging[a]	Discharging[b]	
Fe550	HCl demineralized	718	423 (175)[c]	58.9
Fe 600	HCl demineralized	575	363 (278)[c]	63.1
Fe 600-PO600	HCl demineralized partial oxidation for 0.5 h at 600 °C	625[b]	353 (270)[c]	56.4
Fe 600-PO450	HCl demineralized partial oxidation for 0.5 h at 450 °C	675	408 (301)[c]	60.4
g-Fe 600-2800	HCl demineralized and graphitization	532	367 (324)[c]	69.0
Fe 670H	HCl demineralized	598	365 (237)[c]	61.0
Fe 670	HCl demineralized	742	431 (277)[c]	58.0
Fe 700	HCl demineralized	493	297 (200)[c]	60.0
CN550	HCl demineralized	1314	852 (45)[c]	64.8
CN650	HCl demineralized	1338	601 (110)[c]	44.9
H-fiber (carbon nanotube)	–	2180	534 (90)[c]	24.5
Brazilian graphite	–	494	321 (300)[c]	65.0

[a] Total charging capacity in the voltage range between 0.0 and 0.3 V vs. Li/Li^+.
[b] Total charging capacity in the voltage range between 0.0 and 0.3 V vs. Li/Li^+.
[c] Discharging capacity in the voltage range between 0.0 and 0.3 V vs. Li/Li^+.

0.0–0.3 V vs. Li/Li^+ suggests that CNFs prepared in this study had some amount of low-crystallinity pyrolytic carbon on the surface which might be formed in the gaseous phase in the reactor and adsorbed on the surface of growing CNFs.

CNFs prepared at 600 °C that kept the platelet arrangement showed a smaller d_{002}, while higher preparation temperatures changed this arrangement into tubular, showing no large change in the graphitization degree. Thus, the graphitization degree of CNFs appears to be controlled by the catalytic effect and by the graphene arrangement of produced CNF during the formation of graphene sheets. Tubular-structure Fe 670 showed the largest total discharge capacity and the most distinct stages, reflecting its well developed graphitic structure. Such charge–discharge capacities are believed to reflect the combinations of staged electrochemical intercalation of reduced lithium ion among the graphite layers and the doping of Li ion in the disordered sites of CNFs.

The second performance of concern is the first cycle coulombic efficiency of the CNF. A fairly large reversible charge was observed with CNF as with graphite. The coulombic efficiency was ≈63% with Fe 600 of the highest graphitization degree with platelet arrangement. All CNFs suffered from more of less low efficiency because of their large surface area (due to their nanosized fiber form). The arrangement of graphene sheets may not have a large influence on the coulombic efficiency.

In addition, the edge surface of the sheet may not largely influence the first cycle coulombic efficiency, as shown in Table 2. The side reaction in the first charge cycle at 0.8–1.2 V vs. Li/Li^+ was observed in both Fe 600 and g-Fe 600-2000 which lost the edge surface through the formation of surface loops. The plateaus show no large difference although they become slightly smaller with the increase of graphitization temperature, indicating again that the edge is not so influential for coulombic efficiency.

The CNFs of the present study showed minor charge–discharge characteristics of non-graphitizable carbon in addition to major behavior as graphite. Both non-graphitizable carbon and graphite were reported to show some characteristic features of charge–discharge. CNFs showed charge–discharge at very low potential which is unique to non-graphitizable carbon [19–21,35,40]. Its very small voids are believed to store highly reduced Li to show such discharge. A discharge plateau at 0.8 V which is characteristic of graphitizable carbon heat-treated below 700 °C was not observed with the present Fe-derived CNFs except for Fe 550. Contribution of non-graphitizable carbon is more emphasized in CNFs prepared below 600 °C, as confirmed by EVS. Non-graphitizable carbon may be formed at lower temperature where the catalyst is not always sufficiently activated. Such a non-graphitizable carbon is removed or converted into a graphitic form by the appropriate partial oxidation or graphitization, respectively, graphite charge–discharge profile being exclusively observed after such treatments. Thus such treatments increased the capacity per weight of CNF.

4.2. Anodic performance of graphitized CNF

The graphitization treatment of Fe 600 CNF in the present study hardly improved the graphitization de-

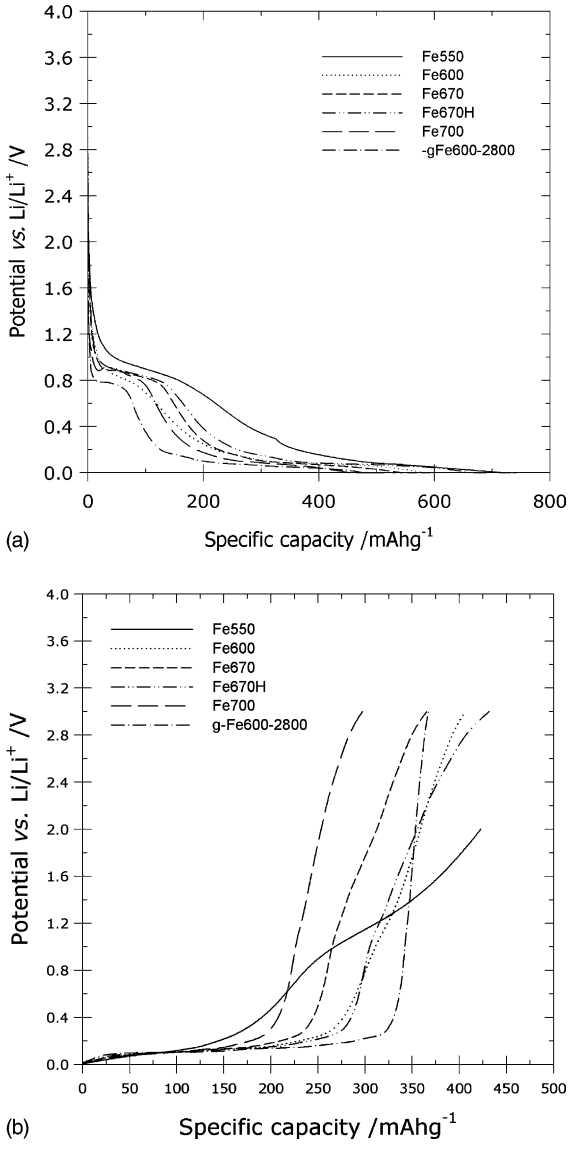

Fig. 5. Galvanostatic (a) charge and (b) discharge profiles of the Fe series.

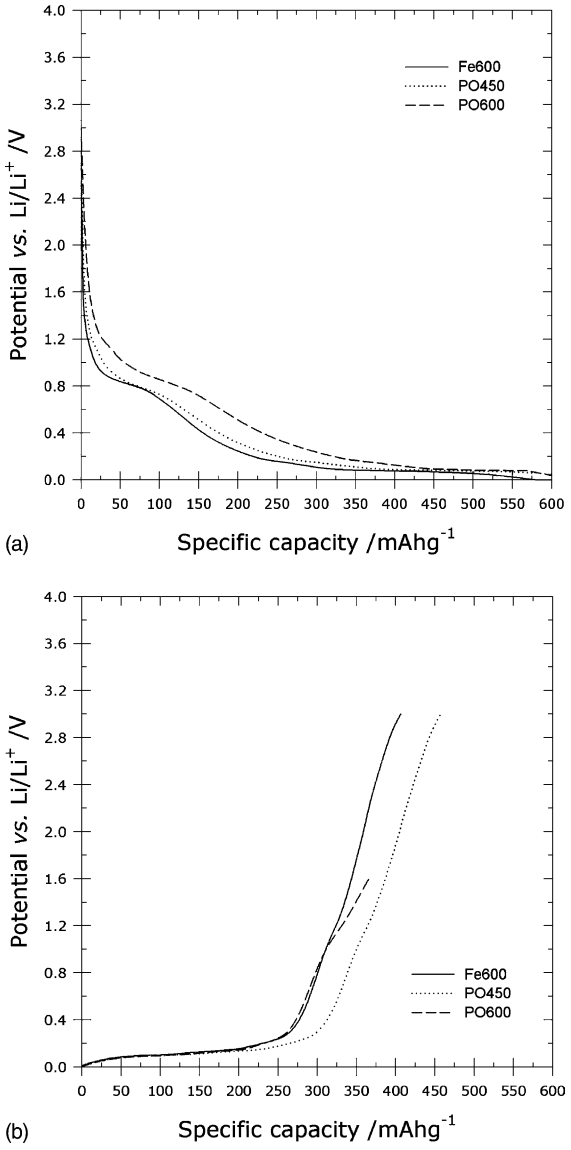

Fig. 6. Galvanostatic (a) charge and (b) discharge profiles of Fe 600, PO450 and PO600.

gree, as indicated by XRD, and slightly increased the capacity. Thus the highest graphitization degree is almost completed by catalytic formation of graphene sheets, although a small amount of non-graphitic carbon was produced at the same time, whose removal does requires a graphitization treatment.

The TEM observation showed a major change of surface alignment of graphene sheets. Many rather uniform loops are induced on the edges of platelet units. The following points are to be noted:

(1) Graphitization forms such loops at the surface of CNF particularly with platelet arrangement.
(2) CNF with loops showed basically the similar extent of first cycle coulombic efficiency.

The edge of a graphene sheet which is perpendicular to the CNF surface is certainly reduced by being covered with loops. The irreversible capacity associated with the edge surfaces of graphite is believed to be substantially larger than that associated with the basal plane surfaces due to solvent co-intercalation into the layer spacing [41]. However, the present study could not find results to confirm such an assumption. The low coulombic efficiency may be induced from another reason, such as the high surface area of these materials.

4.3. Staging phenomena

The graphite intercalation stage or insertion phenomena have been studied previously [8,39,42–44].

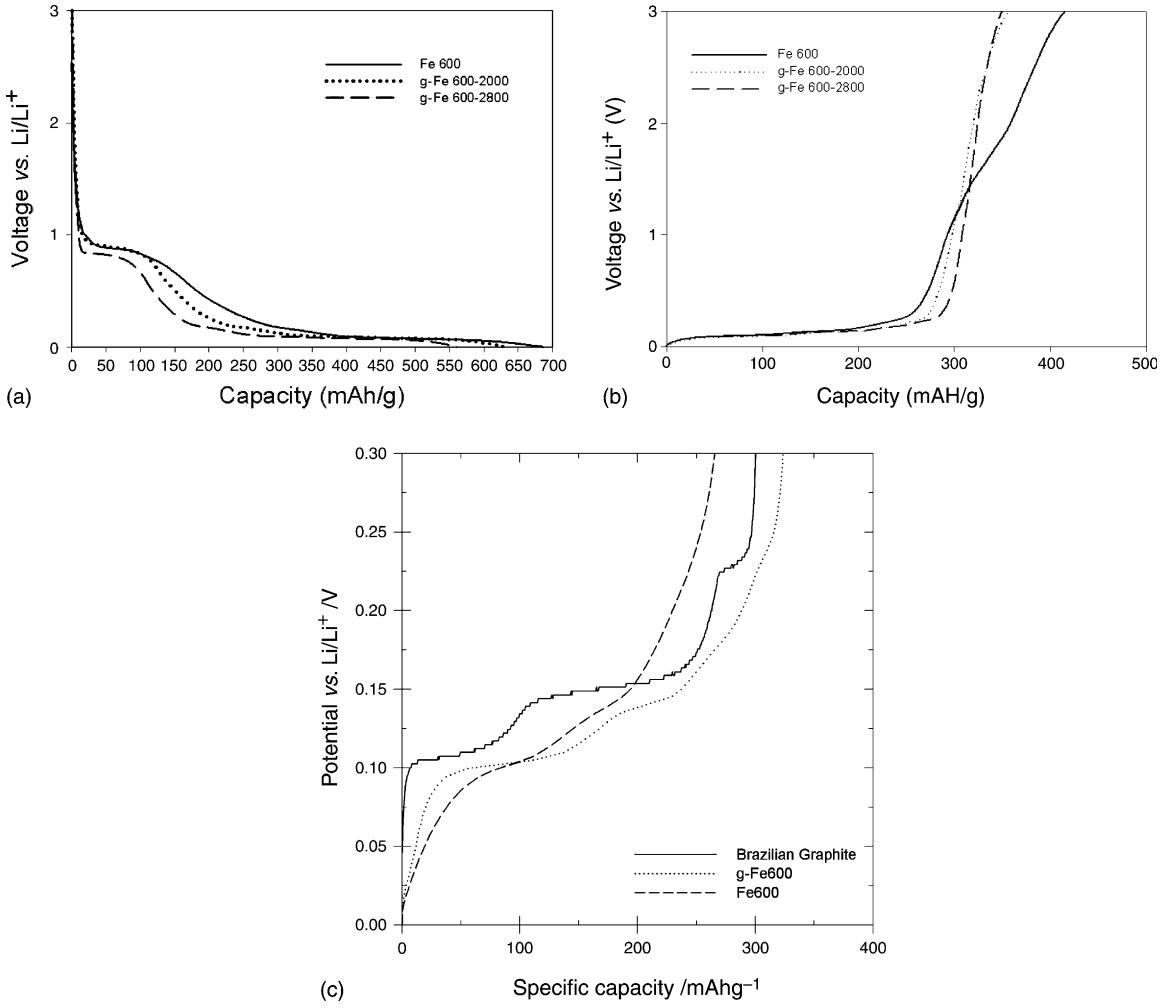

Fig. 7. Galvanostatic charge–discharge profiles of the Fe 600, graphitized Fe-600s at 2000 and 2800 °C, and Brazilian graphite (BG).

Dahn and co-workers [39,42] reported that Lonza KS 44, an artificial graphite, gave five distinguishable peaks in the slow scan differential chronopotentiograms, while three peaks were observed with Brazilian graphite in this work, although five peaks were observed with g-Fe 600-2800. The EVS peaks labeled B, C and E commonly observed with graphite are assigned based on the literature: B, a coexistence of stages 1 and 2; C, a coexistence of stages 2 and 2L (liquid-like stage 2); and E, a coexistence of stages 4 and 1′ (dilute stage 1).

The peak labeled D may be accounted as intercalation into turbostratic disordered layers [35,45,46]. It is interesting to note that natural graphite, such as Brazilian graphite studied in this work, gives three distinct peaks in the discharge EVS profiles, whereas four or five are observed in the case of artificial graphite such as Lonza KS 44 and needle coke-derived carbons [35,45]. The turbostratic peak may appear only in the less graphitized artificial ones. In general, graphitized material is composed of well-ordered graphitic layers with some turbostratically disordered layers that are stacked with some translational and rotational disorder between the adjacent graphitic interlayers. As the graphitization proceeds, the disordered region is converted to more ordered layers. Brazilian graphite, which has a high graphitization degree, did not show peak D.

The peak labeled A is found only in less graphitized materials and disappears with further graphitization or partial oxidation. Thus it is suspected to be associated with a particular amorphous carbon, e.g., thermosetting polymer or pitch derived hard carbons.

4.4. CNF as candidate for commercial graphite anode of lithium ion battery

The high graphitization degree of CNFs obtained at temperatures as low as 670 °C appears to promise high capacity as anode in lithium ion secondary battery. Optimized conditions of CNF preparation can further improve their graphitization degree and capacity. The very thin diameter of CNF promises a fundamentally better cycle stability and rapid charge–discharge, be-

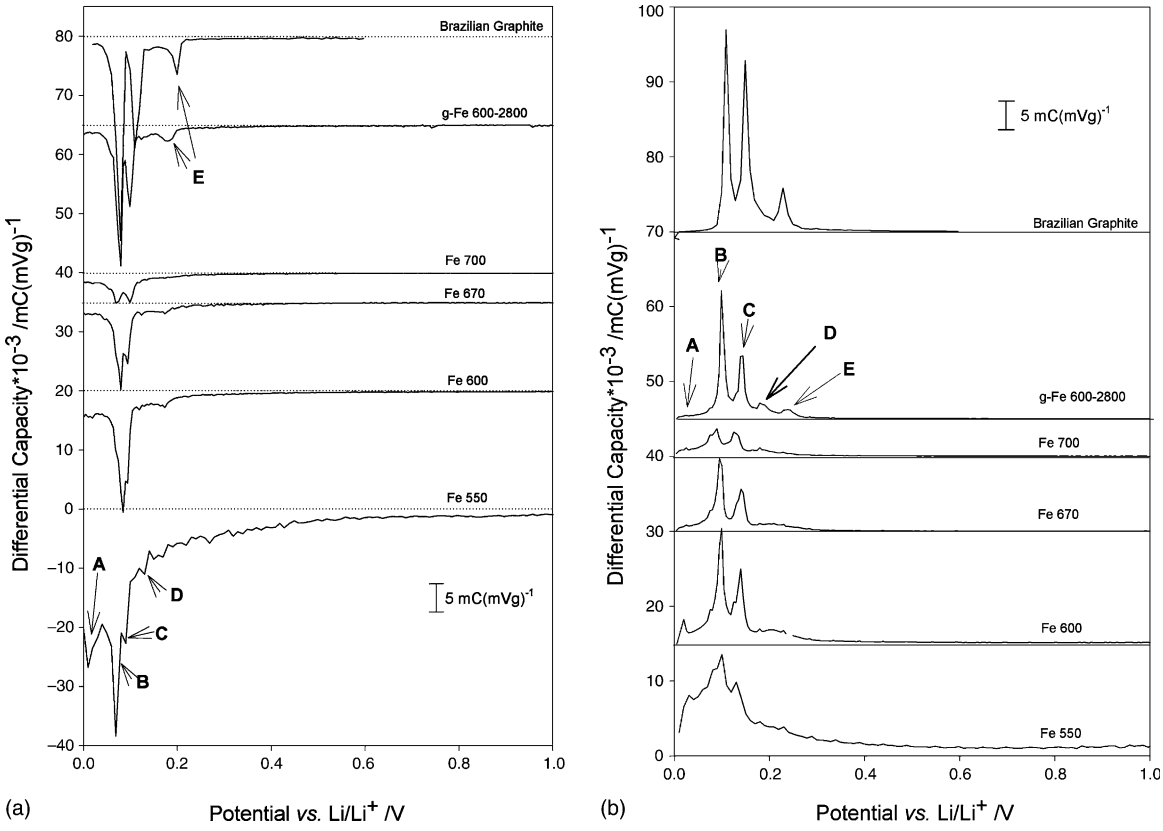

Fig. 8. (a) Charge and (b) discharge EVS profiles of the Fe series and Brazilian graphite (BG). The measurement was made with an $I_{threshold}$ of 0.02 mA in the potential range of 0.0–1.0 V (vs. Li/Li^+).

cause of small stress and rapid intercalation–deintercalation due to this small dimension. The main problem is the low coulombic efficiency, presumably due to the large surface. The surface of carbon grains in the anode where Li ion meets first with the graphitic structure may cause the reaction of lithium and electrolyte. Hence, forming of CNF into a grain covered with suitable carbon from the binder may solve the efficiency problem. Such an approach may preserve the advantages of the CNFs in cycle stability and charge–discharge rate by controlling the packing density and arrangement of filaments. Improvement of the electrolyte must also be achieved for better overall performance.

In conclusion, CNF is a promising carbon and an efficient material for lithium ion battery anode when its mass production and adequate control of its structure are achieved.

Acknowledgements

This research was performed by the financial support of '*Center for Nanostructured Materials Technology*' under '*21st Century Frontier R&D Programs*' of the Ministry of Science and Technology, Korea.

References

[1] Wakihara M. Recent developments in lithium ion batteries. Mat Sci Eng R-Rep 2001;33(4):109–34.
[2] Dahn JR, Sleigh AK, Shi H, Way BM, Weydanz WJ, Reimers JN, et al. New materials, development perspectives. In: Pistoia G, editor. Lithium Batteries. London: Elsevier Science; 1995. p. 1.
[3] Fong R, VonSacken U, Dahn JR. Studies of lithium intercalation into carbons using nonaqueous electrochemical-cells. J Electrochem Soc 1990;137(7):2009–13.
[4] Dahn JR, Zheng T, Liu Y, Xue JS. Mechanisms for lithium insertion in carbonaceous materials. Science 1995;270(5236):590–3.
[5] Mabuchi A, Takumitsu K, Fujimoto H, Kasuh T. Charge–discharge characteristics of the mesocarbon microbeads heat-treated at different temperatures. J Electrochem Soc 1995;142(4):1041–6.
[6] Takami N, Satoh A, Hara M, Ohsaki T. Rechargeable lithium-ion cells using graphitized mesophase-pitch-based carbon fiber anodes. J Electrochem Soc 1995;142(8):2564–71.
[7] Iijima T, Suzuki K, Matsuda Y. Electrodic characteristics of various carbon materials for lithium rechargeable batteries. Synthet Met 1995;73(1):9–20.
[8] Ohzuku T, Iwakoshi Y, Sawai K. Formation of lithium–graphite intercalation compounds in nonaqueous electrolytes and their application as a negative electrode for a lithium ion (shuttlecock) cell. J Electrochem Soc 1993;140(9):2490–8.
[9] Shu ZX, McMillan RS, Murray JJ. Electrochemical intercalation of lithium into graphite. J Electrochem Soc 1993;140(4):922–7.

[10] Tran TD, Spellman LM, Goldberger WM, Song X, Kinoshita K. Lithium intercalation in heat-treated petroleum cokes. J Power Sources 1997;68(1):106–9.
[11] Kostecki R, Tran T, Song X, Kinoshita K, McLarnon F. Raman spectroscopy and electron microscopy of heat-treated petroleum cokes for lithium-intercalation electrodes. J Electrochem Soc 1997;144(9):3111–7.
[12] Jean M, Tranchant A, Messina R. Reactivity of lithium intercalated into petroleum coke with carbonate electrolytes. J Electrochem Soc 1996;143(2):391–4.
[13] Sonobe N, Ishikawa M, Iwasaki T. Development of carbon materials as anode material for lithium ion secondary battery. In: The Extended Abstracts of the 35th Battery Symposium in Japan, The Committee of Battery Technology, The Electrochemical Society of Japan, November 14–16, 1994. p. 47–8.
[14] Dahn JR, Sleigh AK, Shi H, Reimers JN, Zhong Q, Way BM. Dependence of the electrochemical intercalation of lithium in carbons on the crystal-structure of the carbon. Electrochim Acta 1993;38(9):1179–91.
[15] Gibaud A, Xue JS, Dahn JR. A small angle X-ray scattering study of carbons made from pyrolyzed sugar. Carbon 1996;34(4):499–503.
[16] Fujimoto H, Mabuchi A, Tokumitsu K, Kasuh T, Akuzawa N. Effect of crystallite size on the chemical-compositions of the stage-1 alkali metal–graphite intercalation compounds. Carbon 1994;32(2):193–8.
[17] Ohzuku T, Iwakoshi Y, Sawai K. Formation of lithium–graphite intercalation compounds in nonaqueous electrolytes and their application as a negative electrode for a lithium ion (shuttlecock) cell. J Electrochem Soc 1993;140(9):2490–8.
[18] Herold A. Recherches sur les composes dinsertion du graphite. B Soc Chim Fr 1955;(7–8):999–1012.
[19] Sato K, Noguchi M, Demachi A, Oki N, Endo M. A mechanism of lithium storage in disordered carbons. Science 1994;264(5158):556–8.
[20] Takahashi Y, Oishi J, Miki Y, Yoshimura M, Shibahara K, Sakamoto H. Characteristics of disordered carbon materials as negative electrodes for lithium rechargeable batteries. In: The Extended Abstracts of the 35th Battery Symposium in Japan, The Committee of Battery Technology, The Electrochemical Society of Japan, November 14–16, 1994. p. 39–40.
[21] Ishikawa M, Sonobe N, Chuman H, Iwasaki T. The study on the states of lithium in nongraphitizable carbon. In: The Extended Abstracts of the 35th Battery Symposium in Japan, The Committee of Battery Technology, The Electrochemical Society of Japan, November 14–16, 1994. p. 49–50.
[22] Rodriguez NM, Kim MS, Baker RTK. Promotional effect of carbon-monoxide on the decomposition of ethylene over an iron catalyst. J Catal 1993;144(1):93–108.
[23] Nalimova VA, Sklovsky DE, Bondarenko GN, Alvergnat Gaucher H, Bonnamy S, Beguin F. Lithium interaction with carbon nanotubes. Synthet Met 1997;88(2):89–93.
[24] Gaucher H, Pellenq R, Bonnamy S, Beguin F, Nalimova V, Grillet Y. In: Kuzmany H, Fink J, Mehring M, Roth S, editors. Molecular nanostructures. 1997. p. 395–8.
[25] Wu GT, Wang CS, Zhang XB, Yang HS, Qi ZF, Li WZ. Lithium insertion into CuO/carbon nanotubes. J Power Sources 1998;75(1):175–9.
[26] Che GL, Lakshmi BB, Fisher ER, Martin CR. Carbon nanotubule membranes for electrochemical energy storage and production. Nature 1998;393(6683):346–9.
[27] Leroux F, Metenier K, Gautier S, Frackowiak E, Bonnamy S, Beguin F. Electrochemical insertion of lithium in catalytic multi-walled carbon nanotubes. J Power Sources 1999;81:317–22.
[28] Wu GT, Wang CS, Zhang XB, Yang HS, Qi ZF, Li WZ. Structure and lithium insertion properties of carbon nanotubes. J Electrochem Soc 1999;146(5):1696–701.
[29] Houska CR, Warren BE. X-ray study of the graphitization of carbon black. J Appl Phys 1954;25(12):1503–9.
[30] Endo M, Nishimura Y, Takahashi T, Takeuchi K, Dresselhaus MS. Lithium storage behavior for various kinds of carbon anodes in Li ion secondary battery. J Phys Chem Solids 1996;57:725–8.
[31] Blayden HE, Gibson J, Riley HL. A study of bituminous coal by A. exhaustive solvent extraction and B. X-ray diffraction. J Chem Soc 1948;(October):1693–700.
[32] Katagiri G. Raman spectroscopy of graphite and carbon materials and its recent application. Tanso 1996;175:304–13.
[33] Thompson AH. Electrochemical potential spectroscopy—new electrochemical measurement. J Electrochem Soc 1979;126(4):608–16.
[34] Conway BE, Thompson AH. Electrochemical potential spectroscopy—discussion. J Electrochem Soc 1980;127(6):1319–20.
[35] Park CW, Yoon SH, Oh SM. Li storage sites in non-graphitizable carbons prepared from methylnaphthalene-derived isotropic pitches. Carbon 2000;38:995–1001.
[36] Park CW, Yoon SH, Oh SM. An EVS (electrochemical voltage spectroscopy) study for the comparison of graphitization behaviors of two petroleum needle cokes. Carbon 2000;38:1261–9.
[37] Best RJ, Russell WW. Nickel, copper and some of their alloys as catalysts for ethylene hydrogenation. J Am Chem Soc 1954;76:838–42.
[38] JSPS (Japan Society for Promotion of Science). On the measurement of lattice parameters and unit cell dimension of artificial graphite. Tanso 1963;36:25–34.
[39] Zheng T, Reimers JN, Dahn JR. Effect of turbostratic disorder in graphitic carbon hosts on the intercalation of lithium. Phys Rev B 1995;51(2):734–41.
[40] Mochida I, Ku C-H, Korai K. Anodic performance and insertion mechanism of hard carbons prepared from synthetic isotropic pitches. Carbon 2001;39:399–410.
[41] Chung G, Jun S, Lee K, Kim M. Effect of surface structure on the irreversible capacity of various graphitic carbon electrodes. J Electrochem Soc 1999;146:1664–71.
[42] Dahn JR, Fong R, Spoon MJ. Suppression of staging in lithium-intercalated carbon by disorder in the host. Phys Rev B 1990;42(10):6424–32.
[43] Daumas N, Herold A. Relations between phase concept and reaction mechanics in graphite insertion compounds. C R Acad Sci C Chim 1969;268(5):373.
[44] Woo KC, Kamitakahara WA, DiVincenzo DP, Robinson DS, Mertwoy H, Milliken JW, et al. Effect of inplane density on the structural and elastic properties of graphite-intercalation compounds. Phys Rev Lett 1983;50(3):182–5.
[45] Tran TD, Feiker JH, Song X, Kinoshita K. Commercial carbonaceous materials as lithium intercalation anodes. J Elecchem Soc 1995;142:3297–302.
[46] Satoh A, Takami N, Ohsaki T. Electrochemical intercalation of lithium into graphitized carbons. Solid State Ion 1995;80(3–4):291–8.